Journal of the Ceramic Society of Japan 126 [11] 920-924 2018
DOI http://doi.org/10.2109/jcersj2.18127

JCS-Japan

FULL PAPER

Magnetic properties of rare earth rhenium oxides Ln_3ReO_7 (Ln = Y, Er–Lu) with fluorite-related structure

Masaki INABAYASHI[1], Yoshihiro DOI[1], Makoto WAKESHIMA[1] and Yukio HINATSU[1,†]

[1] Division of Chemistry, Graduate School of Science, Hokkaido University, Sapporo 060–0810, Japan

Ternary rare earth rhenium oxides Ln_3ReO_7 (Ln = Y, Er–Lu) have been prepared. Their X-ray diffraction measurements and the Rietveld analysis show that these compounds have an orthorhombic superstructure of fluorite-type with space group $C222_1$ (for Ln = Y, Er, Tm) or a defect-fluorite structure $Fm\bar{3}m$ (for Ln = Yb, Lu). The zero-field-cooling and field-cooling magnetic susceptibility for Y_3ReO_7 diverse when the temperature is decreased through 10 K. At the same temperature, specific heat anomaly is also observed. The results of the specific heat measurements for Tm_3ReO_7 and Yb_3ReO_7 indicate the existence of magnetic anomaly below 7 and 2.2 K, respectively. On the other hand, Er_3ReO_7 and Lu_3ReO_7 are paramagnetic down to 1.8 K.

Key-words : Magnetic properties, Rare earth, Rhenium, Oxides, Fluorite-related structure

[Received June 21, 2018; Accepted August 10, 2018]

1. Introduction

The solid state chemistry of mixed-metal oxides containing both rare earths (4*f* metals) and 4*d* or 5*d* transition metals has attracted a great deal of interest. These materials adopt a diverse range of structures and show a wide range of electronic properties due to 4*f* and 4*d* (or 5*d*) electrons. Among many compounds, the structural chemistry and magnetic properties of compounds with general formula Ln_3MO_7 (Ln = rare earths, M = 4*d* or 5*d* transition metals) have been attracting interest. The structure most found for Ln_3MO_7 is an orthorhombic superstructure of the fluorite-type (lattice parameter a_f) with space group *Cmcm* and unit-cell parameters $a_{orth} \approx 2a_f$, $b_{orth} \approx c_{orth} \approx \sqrt{2}\, a_f$.[1)] There are three distinct cation sites, one distorted cubic Ln^{3+} site, one distorted pentagonal bipyramidal Ln^{3+} site and one octahedral M^{5+} site. The M^{5+} cation is octahedrally coordinated by six oxygen ions and the octahedra share corners forming a zig-zag chain parallel to the *c*-axis. In this structure, slabs are formed in the *bc*-plane, in which one-dimensional MO_6 chain runs parallel to the *c*-axis alternating with rows of edge-shared LnO_8 pseudo-cubes consisting of one-third of Ln ions. These slabs are separated by the remaining two thirds of Ln ions which is seven-coordinated by oxygen ions. The interchain *M*–*M* distance is about 6.6 Å compared with the corresponding intrachain distance of 3.7 Å, which suggests that these compounds may exhibit one-dimensional electronic behavior. In addition, since most of the lanthanides have a nonzero spin, this could lead to long-range order due to *Ln*–*M* coupling at some finite temperatures.

Due to this unique crystal structures and possible related magnetic properties, many studies have been performed,[2)–40)] especially for the magnetic properties of compounds containing Ru at the *M*-site.[2)–12)] Recently, detailed magnetic and thermal investigations were reported for the ruthenium-, iridium- and osmium-containing members of the Ln_3MO_7 family and provided evidence for the existence of low-temperature structural phase transitions.[8)–10),12),17),18),20),28)]

As for rhenium-containing compounds, Wltschek et al. first determined the crystal structure of Sm_3ReO_7 to be orthorhombic with space group *Cmcm*.[27)] After that, many studies on the structure and magnetic properties of Ln_3ReO_7 (Ln = Pr, Nd, Sm–Ho) were reported.[13)–15)] They crystallize in an orthorhombic superstructure of fluorite (space group *Cmcm* for Ln = Pr, Nd, Sm–Tb; $C222_1$ for Ln = Ho). Most of these compounds show a magnetic anomaly at low temperatures (1.9–14 K), but no trend between its temperatures and rare earths is observed.

In this study, we extended the preparation of Ln_3ReO_7 to Ln = Y, Er–Lu. Through X-ray diffraction measurements, their crystal structures were determined. The magnetic susceptibility and specific heat measurements were performed from 1.8 to 400 K in order to elucidate their magnetic properties.

2. Experimental

2.1 Sample preparation

Samples were prepared by the solid state reaction. As starting materials, Ln_2O_3, ReO_2, and ReO_3 were used. They were weighed in an appropriate metal ratio and were ground in an agate mortar. The mixtures were pelletized and sealed in an evacuated platinum tube, and then heated at 1350–1400°C for 6–12 h. With several intermediate re-

† Corresponding author: Y. Hinatsu; E-mail: hinatsu@sci.hokudai.ac.jp

grindings and re-pelletizing, the products were annealed at the same temperature until a single Ln_3ReO_7 phase was obtained.

2.2 X-ray diffraction analysis

Powder X-ray diffraction measurements were performed in the region of $10° \leq 2\theta \leq 120°$ using Cu K_α radiation on a Rigaku MultiFlex diffractometer equipped with a curved graphite monochromator. The X-ray diffraction data were analyzed by the Rietveld technique, using the programs RIETAN-FP,[41] and the crystal structure was drawn by using the VESTA program.[42]

2.3 Magnetic susceptibility measurements

The temperature-dependence of the magnetic susceptibility was measured in an applied field of 0.1T over the temperature range of $1.8\,K \leq T \leq 400\,K$, using a SQUID magnetometer (Quantum Design, MPMS5S). The susceptibility measurements were performed under both zero-field-cooling (ZFC) and field-cooling (FC) conditions. The former was measured upon heating the sample to 400 K under the applied magnetic field of 0.1 T after zero-field cooling to 1.8 K. The latter was measured upon cooling the sample from 400 to 1.8 K at 0.1 T.

2.4 Specific heat measurements

The specific heat measurements were carried out using a relaxation technique with a commercial physical property measurement system (Quantum Design) in the temperature range of $1.8\,K \leq T \leq 300\,K$. The pelletized sample (~10 mg) was mounted on a thin alumina plate with Apiezon N-grease for better thermal contact.

3. Results and discussion

3.1 Preparation and crystal structure

The results of X-ray diffraction measurements show that Ln_3ReO_7 (Ln = Y, Er–Lu) could be prepared as single-phase compounds. In the preparation process, very small amounts of impurities remained in the desired compounds; they were unreacted starting materials Ln_2O_3. This is presumably a consequence of the loss of more volatile rhenium oxides. In order to remove these impurities, the samples were washed with diluted hydrochloric acid.

Figures 1(a) and 1(b) show the X-ray diffraction profiles for Y_3ReO_7 and Yb_3ReO_7, respectively. Previous studies indicate that Ln_3ReO_7 compounds have the orthorhombic structure with space group *Cmcm* (for Ln = Pr, Nd, Sm–Tb) or $C222_1$ (for Ln = Dy, Ho).[13)–15)] Since the ionic radii of Y, Er and Tm are smaller than that of Dy, we analyzed the crystal structure of Ln_3ReO_7 (Ln = Y, Er, Tm) with the same space group $C222_1$. In the X-ray diffraction profiles for Y_3ReO_7, Er_3ReO_7, and Tm_3ReO_7, there exist many very weak *h0l* reflections with odd *l* (e.g. the peak at 2θ~20.4° corresponding to the 2 0 1 reflection), which cannot be indexed based on the *Cmcm*. All the reflections observed for Ln_3ReO_7 (Ln = Y, Er, Tm) could be successfully indexed with space group $C222_1$. **Table 1** lists the lattice parameters and atomic coordinates for

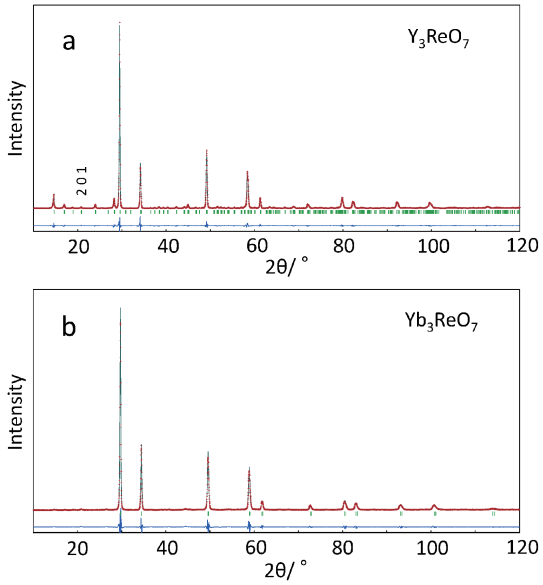

Fig. 1. Powder X-ray diffraction profiles for (a) Y_3ReO_7 and (b) Yb_3ReO_7. The calculated and observed profiles are shown on the top solid line and cross markers, respectively. The vertical marks in the middle show positions calculated for Bragg reflections. The lower trace is a plot of the difference between calculated and observed intensities.

Table 1. Structural parameters for Y_3ReO_7

Atom	Site	*x*	*y*	*z*	B/Å^2
Y(1)	4*b*	0	0.496(1)	1/4	0.95(4)
Y(2)	8*c*	0.235(1)	0.237(2)	0	0.59(3)
Re	4*b*	0	0	1/4	0.64(2)
O(1)	8*c*	0.146(2)	0.180(2)	0.295(3)	1.11(2)
O(2)	8*c*	0.112(2)	0.756(2)	0.266(3)	1.11
O(3)	4*a*	0.136(2)	1/2	0	1.11
O(4)	4*a*	0.147(2)	1/2	1/2	1.11
O(5)	4*a*	0.071(1)	0	0	1.11

Note. Space group $C222_1$; $a = 10.4422(5)$ Å, $b = 7.4149(6)$ Å, $c = 7.4123(4)$ Å, $V = 473.92(6)$ Å^3, $R_{wp} = 11.88\%$, where

$$R_{wp} = \left\{ \sum_i w_i [y_i - f_i(x)]^2 / \sum_i w_i y_i^2 \right\}^{1/2}.$$

a: For oxygen ions, *B* values were fixed to be equal.

Y_3ReO_7. The Ln_3ReO_7 (Ln = Yb, Lu) show simple X-ray diffraction patterns indexed with a cubic cell of the fluorite-type structure [see Fig. 1(b)]. In this structure, the *Ln* and Re ions randomly occupy the cation site (4*a* site in the space group $Fm\bar{3}m$) in the ratio of 3:1, and 1/8 of the oxide ions are randomly defective at the anion site (4*b* site); more properly, their formula unit can be represented as $Ln_{0.75}Re_{0.25}O_{1.75}$. **Table 2** lists the lattice parameters and atomic coordinates for Yb_3ReO_7.

Figure 2 illustrates the schematic crystal structures for Ln_3ReO_7 with space groups $C222_1$ (for Ln = Y, Dy–Tm). In the orthorhombic structures, the ReO_6 octahedra share the O(5) ions and form an infinite one-dimensional zig-zag chain parallel to the [001] direction. The Ln(1) ions are coordinated by eight oxygen ions and the distorted $Ln(1)O_8$ cubes also form an one-dimensional chain through edge-sharing. The ReO_6 and $Ln(1)O_8$ chains lie

Table 2. Structural parameters for Yb_3ReO_7

Atom	Site	occupancy	x	y	z	B/Å^2
Yb	4*a*	0.75	0	0	0	1.56(3)
Re	4*a*	0.25	0	0	0	1.56
O	4*b*	0.875	1/4	1/4	1/4	5.39(2)

Note. Space group $Fm\bar{3}m$; $a = 5.1950(2)$ Å, $V = 140.20(1)$ Å^3, $R_{wp} = 12.73\%$.

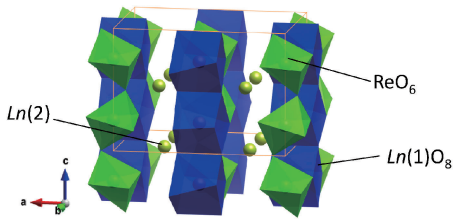

Fig. 2. Schematic crystal structures of Ln_3ReO_7 (Ln = Y, Dy–Tm, space group: $C222_1$).

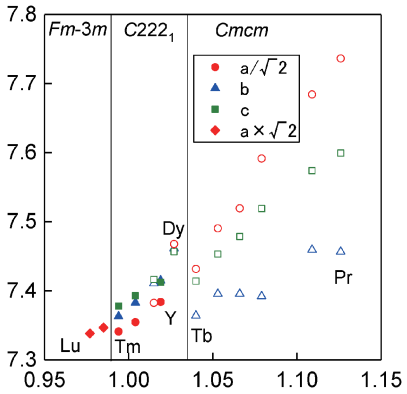

Fig. 3. Variation of lattice parameters for Ln_3ReO_7 with ionic radius of eight-coordinate Ln^{3+} ions. Open symbols correspond to lattice parameters for Ln = Pr, Nd, Sm–Ho compounds with *Cmcm* or $C222_1$ space group previously reported.

alternately parallel to the (010) plane, and the Ln(2) ions are seven-coordinated by oxygen ions between the slabs consisting of these chains.

Figure 3 shows the variation of lattice parameters for Ln_3ReO_7 (Ln = Y, Er–Lu) against the ionic radii of the 8-coordinate Ln^{3+} ions.[43] The lattice parameter data for Ln_3ReO_7 (Ln = Pr, Nd, Sm–Ho) reported previously[14),15)] are also included in this figure. For comparison, all the data are converted to $\sqrt{2}a_f$. The lattice parameters tend to increase smoothly with the ionic radius of Ln^{3+} ions. This result also indicates that all the rare earth ions are in the trivalent state in these Ln_3ReO_7 compounds.

3.2 Magnetic properties

3.2.1 Y_3ReO_7

Figure 4(a) shows the temperature dependence of the magnetic susceptibilities for Y_3ReO_7 in the temperature range of 1.8–300 K. Below 10 K, a divergence between the ZFC and FC magnetic susceptibilities has been observed. Figure 4(b) shows the temperature dependence of the specific heat divided by temperature (C_p/T) for Y_3ReO_7 in the temperature range of 1.8–30 K. A specific heat anomaly

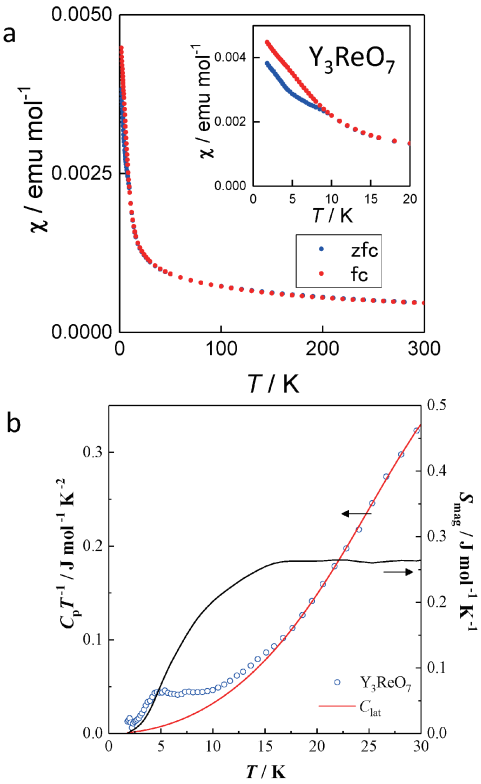

Fig. 4. (a) Temperature dependence of the magnetic susceptibility for Y_3ReO_7 in the temperature range from 1.8 to 300 K. The inset shows the detailed magnetic susceptibility vs. temperature curve below 20 K. (b) Temperature dependence of specific heat divided by temperature (C_p/T) and magnetic entropy change (S_{mag}) for Y_3ReO_7 below 30 K.

has been observed at the same temperature at which the ZFC and FC susceptibilities begin to diverse. Since the Y^{3+} ion is diamagnetic, these magnetic anomalies are due to the magnetic behavior of Re^{5+} ions. Similar magnetic anomaly has been also found for Eu_3ReO_7 in which Eu^{3+} ions are nonmagnetic.[15] The Curie–Weiss relationship has been found for the susceptibility above 100 K, and the effective magnetic moment and the Weiss constant are obtained to be 1.00 μ_B and −125 K, respectively. The negative Weiss constant indicates that the predominant magnetic interaction at low temperatures is antiferromagnetic. The effective magnetic moment is smaller than the theoretical moment from spin-only for Re^{5+} (2.83 μ_B), which is due to the effect of the crystal field. Similar results have been observed in some Ln_3ReO_7 compounds[14),15)] and Re^{5+}-containing compounds.[44),45)]

In the following, we will evaluate the magnetic specific heat for Y_3ReO_7. The magnetic specific heat (C_{mag}) was estimated by extracting the lattice specific heat (C_{lat}) from the total specific heat (C_p). The C_{lat} was calculated from the sum of the Debye and Einstein models:[46]

$$C_{lat} = 9R\left(\frac{T}{\theta_D}\right)^3 \int_0^{\theta_D/T} \frac{(\theta_D/T)^4 e^{\theta_D/T}}{(e^{\theta_D/T}-1)^2} d(\theta_D/T) + R\sum_{i=1}^{3} \frac{(\theta_{E_i}/T)^2 e^{\theta_{E_i}/T}}{(e^{\theta_{E_i}/T}-1)^2}$$

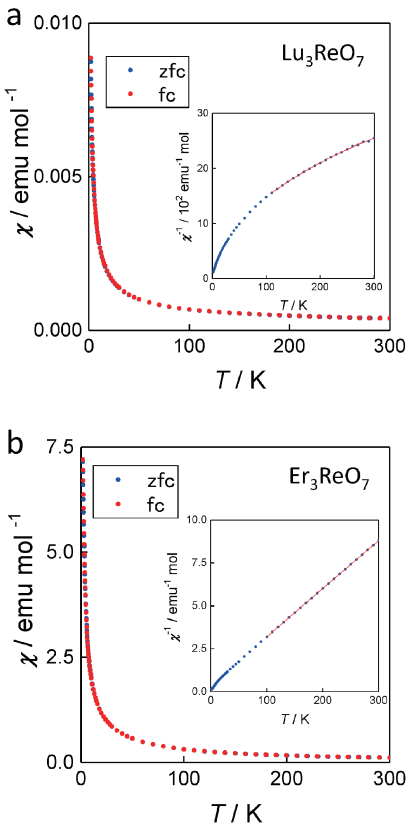

Fig. 5. (a) Temperature dependence of the magnetic susceptibility for Lu_3ReO_7 in the temperature range from 1.8 to 300 K. The inset shows the reciprocal susceptibility vs. temperature curve. The red solid line is the Curie–Weiss fitting. (b) Temperature dependence of the magnetic susceptibility for Er_3ReO_7 in the temperature range from 1.8 to 300 K. The inset shows the reciprocal susceptibility vs. temperature curve. The red solid line is the Curie–Weiss fitting.

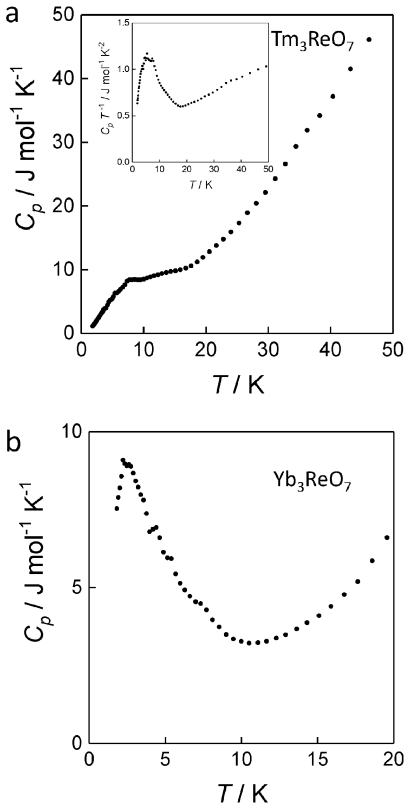

Fig. 6. (a) Temperature dependence of the specific heat (C_p) for Tm_3ReO_7 below 50 K. The inset shows the specific heat divided by temperature (C_p/T). (b) Temperature dependence of the specific heat (C_p) for Yb_3ReO_7 below 20 K.

where θ_D and θ_{Ei} are the Debye and Einstein temperatures, respectively. The calculated C_{lat} curve is shown as a red dotted line in Fig. 4(b). From the temperature dependence of the magnetic specific heat, the magnetic entropy change (S_{mag}) due to the magnetic ordering observed for Y_3ReO_7 is calculated by the relation $S_{mag} = \int (C_{mag}/T)dT$. The temperature dependence of the S_{mag} is also shown in Fig. 4(b). The magnetic entropy change for Y_3ReO_7 is about 0.3 $J\,mol^{-1}\,K^{-1}$.

The electron configuration of the Re^{5+} ion is $[Xe]5d^2$ (the state $^3F_2$, [Xe]: Xenon electronic core), and the ground state is $S = 1$. Therefore, the magnetic entropy change for Re^{5+} is calculated to be $R\ln(2S+1) = 9.13\,J\,mol^{-1}\,K^{-1}$, where R and S are the molar gas constant and the spin quantum number, respectively. The magnetic entropy change experimentally determined from specific heat measurements is much smaller than this estimated value. At present, the reason for this is not clear.

3.2.2 Lu_3ReO_7 and Er_3ReO_7

Figure 5(a) shows the temperature dependence of the magnetic susceptibilities for Lu_3ReO_7 in the temperature range of 1.8–300 K. No divergence between the ZFC and FC magnetic susceptibilities has been observed in the experimental temperature range. Specific heat measurements also indicate that Lu_3ReO_7 is paramagnetic in the experimental temperature range and no magnetic anomaly has been detected down to 1.8 K. From the Curie–Weiss fitting to the susceptibility above 100 K, the effective magnetic moment and the Weiss constant are obtained to be 0.78 μ_B and −53.8 K, respectively. The smaller effective magnetic moment than the theoretical moment indicates that this is due to the effect of the crystal field.

Figure 5(b) shows the temperature dependence of the magnetic susceptibility for Er_3ReO_7. No magnetic ordering has been observed down to 1.8 K. The Curie–Weiss relationship has been found for the susceptibility above 100 K [see the inset of Fig. 5(b)], and the effective magnetic moment and the Weiss constant are obtained to be 16.7 μ_B and −11.6 K, respectively. Since the theoretical effective magnetic moments for Er^{3+} and Re^{5+} are 9.59 and 2.83 μ_B, respectively, the effective magnetic moment for Er_3ReO_7 μ_{calc} is calculated to be 16.8 μ_B from the equation $\mu_{calc} = \sqrt{3\mu_{Er^{3+}}{}^2 + \mu_{Re^{5+}}{}^2}$. The moment obtained from the experiment is in good agreement with this value.

3.2.3 Tm_3ReO_7 and Yb_3ReO_7

Figures 6(a) and 6(b) show the temperature dependence of the specific heat at low temperatures for Tm_3ReO_7 and Yb_3ReO_7, respectively. The specific data for these compounds indicate the occurring of magnetic ordering at 7 and 2.2 K, respectively.

4. Summary

Ln_3ReO_7 (Ln = Y, Er–Lu) crystallized in an orthorhombic superstructure of fluorite-type with space group $C222_1$ (for Ln = Y, Er, Tm) or a defect-fluorite structure $Fm\bar{3}m$ (for Ln = Yb, Lu). Y_3ReO_7 shows a magnetic anomaly below 10 K. The results of the specific heat measurements for Tm_3ReO_7 and Yb_3ReO_7 also indicate the existence of magnetic anomaly below 7 and 2.2 K, respectively. On the other hand, Er_3ReO_7 and Lu_3ReO_7 are paramagnetic down to 1.8 K.

Acknowledgements This study was partly supported by Advanced Physical Property Open Unit (APPOU), Hokkaido University.

References

1) H. J. Rossell, *J. Solid State Chem.*, 27, 115–122 (1979).
2) F. P. F. van Berkel and D. J. W. IJdo, *Mater. Res. Bull.*, 21, 1103–1106 (1986).
3) W. A. Groen, F. P. F. van Berkel and D. J. W. IJdo, *Acta Crystallogr. C*, 43, 2262–2264 (1986).
4) A. Kahn-Harari, L. Mazerrolles, D. Michel and F. Robert, *J. Solid State Chem.*, 116, 103–106 (1995).
5) P. Khalifah, R. W. Erwin, J. W. Lynn, Q. Huang, B. Batlogg and R. J. Cava, *Phys. Rev. B*, 60, 9573–9578 (1999).
6) F. Wiss, N. P. Raju, A. S. Wills and J. E. Greedan, *Int. J. Inorg. Mater.*, 2, 53–59 (2000).
7) B. P. Bontchev, A. J. Jacobson, M. M. Gospodinov, V. Skumryev, V. N. Popov, B. Lorenz, R. L. Meng, A. P. Litvinchuk and M. N. Iliev, *Phys. Rev. B*, 62, 12235–12240 (2000).
8) D. Harada and Y. Hinatsu, *J. Solid State Chem.*, 158, 245–253 (2001).
9) D. Harada, Y. Hinatsu and Y. Ishii, *J. Phys.-Condens. Mat.*, 13, 10825–10836 (2001).
10) D. Harada and Y. Hinatsu, *J. Solid State Chem.*, 164, 163–168 (2002).
11) R. Lam, F. Wiss and J. E. Greedan, *J. Solid State Chem.*, 167, 182–187 (2002).
12) W. R. Gemmill, M. D. Smith and H.-C. zur Loye, *Inorg. Chem.*, 43, 4254–4261 (2004).
13) R. Lam, T. Langet and J. E. Greedan, *J. Solid State Chem.*, 171, 317–323 (2002).
14) Y. Hinatsu, M. Wakeshima, N. Kawabuchi and N. Taira, *J. Alloy. Compd.*, 374, 79–83 (2004).
15) M. Wakeshima and Y. Hinatsu, *J. Solid State Chem.*, 179, 3575–3581 (2006).
16) J. R. Plaisier, R. J. Drost and D. J. W. IJdo, *J. Solid State Chem.*, 169, 189–198 (2002).
17) W. R. Gemmill, M. D. Smith, Y. A. Mozharivsky, G. J. Miller and H.-C. zur Loye, *Inorg. Chem.*, 44, 7047–7055 (2005).
18) Y. Hinatsu and Y. Doi, *J. Solid State Chem.*, 198, 176–185 (2013).
19) R. Morrow, M. A. Susner, M. D. Sumption and P. M. Woodward, *Phys. Rev. B*, 92, 134402 (2015).
20) H. Nishimine, M. Wakeshima and Y. Hinatsu, *J. Solid State Chem.*, 177, 739–744 (2004).
21) Y. Hinatsu, Y. Doi, H. Nishimine, M. Wakeshima and M. Sato, *J. Alloy. Compd.*, 488, 541–545 (2009).
22) M. Wakeshima, D. Harada and Y. Hinatsu, *J. Alloy. Compd.*, 287, 130–136 (1999).
23) J. E. Greedan, N. P. Raju, A. Wegner, P. Gougeon and J. Padiou, *J. Solid State Chem.*, 129, 320–327 (1997).
24) H. Nishimine, M. Wakeshima and Y. Hinatsu, *J. Solid State Chem.*, 178, 1221–1229 (2005).
25) Y. Doi, M. Wakeshima and Y. Hinatsu, *J. Mater. Chem.*, 11, 3135–3140 (2001).
26) N. Ishizawa, K. Tateishi, S. Kondo and T. Suwa, *Inorg. Chem.*, 47, 558–566 (2008).
27) G. Wltschek, H. Paulus, I. Svoboda, H. Ehrenberg and H. Fuess, *J. Solid State Chem.*, 125, 1–4 (1996).
28) Y. Hinatsu and Y. Doi, *J. Solid State Chem.*, 220, 22–27 (2014).
29) J. F. Vente, R. B. Helmholdt and D. J. W. IJdo, *J. Solid State Chem.*, 108, 18–23 (1994).
30) M. Wakeshima, H. Nishimine and Y. Hinatsu, *J. Phys. Condens. Matter*, 16, 4103–4120 (2004).
31) J. F. Vente and D. J. W. IJdo, *Mater. Res. Bull.*, 26, 1255–1262 (1991).
32) M. Inabayashi, Y. Doi, M. Wakeshima and Y. Hinatsu, *J. Solid State Chem.*, 250, 100–106 (2017).
33) M. Inabayashi, Y. Doi, M. Wakeshima and Y. Hinatsu, *J. Solid State Chem.*, 254, 150–154 (2017).
34) Y. Hinatsu and Y. Doi, *J. Solid State Chem.*, 182, 1694–1699 (2009).
35) N. Barrier and P. Gougen, *Acta Crystallogr. E*, 59, i22–i24 (2003).
36) N. Barrier and P. Gougen, *Acta Crystallogr. C*, 63, i102–i104 (2003).
37) M. Wakeshima and Y. Hinatsu, *J. Solid State Chem.*, 183, 2681–2688 (2010).
38) Y. Doi, Y. Harada and Y. Hinatsu, *J. Solid State Chem.*, 182, 709–715 (2009).
39) Y. Hinatsu and Y. Doi, *J. Solid State Chem.*, 217, 16–21 (2014).
40) Y. Hinatsu and Y. Doi, *J. Solid State Chem.*, 239, 214–219 (2016).
41) F. Izumi and K. Momma, *Solid State Phenom.*, 130, 15–20 (2007).
42) K. Momma and F. Izumi, *Appl. Crystallogr*, 41, 653–658 (2008).
43) R. D. Shannon, *Acta Crystallogr.*, A32, 751–767 (1976).
44) Y. Sasaki, Y. Doi and Y. Hinatsu, *J. Mater. Chem.*, 12, 2361–2366 (2002).
45) A. Nishiyama, Y. Doi and Y. Hinatsu, *J. Solid State Chem.*, 248, 134–141 (2017).
46) G. Grimvall, "Thermophysical Properties of Materials in Selected Topics in Solid State Physics"; Elsevier/North-Holland: New York, Vol. 13 (1986) pp. 65–115.